4D Surface Mesh Reconstruction from Segmented Cardiac Images using Subdivision Surfaces

Xi Wang
University of Calgary
Calgary, Canada
xi.wang1@ucalgary.ca

Kathleen D. Ang
University of Calgary
Calgary, Canada
kdang@ucalgary.ca

Faramarz F. Samavati
University of Calgary
Calgary, Canada
samavati@ucalgary.ca

ABSTRACT

With the advances in cardiovascular imaging technologies in recent years, 4D (3D+time) patient-specific modeling of the heart has attracted many research interests. Computational modeling approaches such as Computational Fluid Dynamics (CFD) and Finite Element (FE) have been increasingly used to quantitatively diagnose and predict cardiovascular diseases. In these methods, the geometrical reconstruction of the heart anatomy is usually an indispensable step. This work presents a robust method for reconstructing time-varying subdivision surfaces from the segmentation masks of cardiac images. We first reconstruct a 3D mesh for the first time step by iteratively fitting an initial mesh based on error and tension terms. Each subsequent time step uses the model from its previous time step as the control mesh for subdivision surface fitting. This method preserves the 1-to-1 vertex correspondence between meshes in different time steps and allows us to control the mesh quality (i.e. resolution, smoothness, and accuracy). Furthermore, in contrast to contour-based algorithms, our method can handle non-trivial topological changes such as holes and tunnels. The method has been tested on 3D and 4D datasets of different modalities (i.e. CT and MRI), resolutions, and chambers. For creating visually appealing results, we show that synthetic textures can be mapped to the 4D reconstruction due to the vertex correspondence. We also quantitatively evaluate the reconstructed 3D meshes in terms of mesh quality and conformity to the data.

CCS CONCEPTS

• **Computing methodologies** → **Shape modeling**; • **Applied computing** → **Life and medical sciences**.

KEYWORDS

heart surface reconstruction, subdivision surface, cardiac images

ACM Reference Format:
Xi Wang, Kathleen D. Ang, and Faramarz F. Samavati. 2021. 4D Surface Mesh Reconstruction from Segmented Cardiac Images using Subdivision Surfaces. In *2021 8th International Conference on Bioinformatics Research and Applications (ICBRA 2021), September 11–13, 2021, Berlin, Germany*. ACM, New York, NY, USA, 7 pages. https://doi.org/10.1145/3487027.3487036

ICBRA 2021, September 11–13, 2021, Berlin, Germany

ACM ISBN 978-1-4503-8426-1/21/09…$15.00
https://doi.org/10.1145/3487027.3487036

1 INTRODUCTION

Cardiovascular disease is the leading cause of death worldwide. Cardiac imaging technologies provide non-invasive ways for the diagnosis, monitoring, and treatment of cardiac diseases. Various imaging technologies such as computed tomography (CT), cardiac magnetic resonance (CMR), single photon emission CT (SPECT), and echocardiography have enabled the acquisition of both 3D and 4D (time-varying) cardiac images for various purposes. With the advances in imaging techniques, the creation of personalized cardiac anatomical models has received much research attention recently [13, 22]. Patient-specific computational modeling and simulation can help us better understand cardiac functions and make clinical predictions. For instance, Computational Fluid Dynamics (CFD) and Finite Element (FE) have been increasingly used to quantitatively analyze the behavior of cardiac blood flow (hemodynamics) [16]. Moreover, personalized heart models are a prerequisite to surgical planning tools such as visual reality (VR) and 3D printing [2]. In these applications, the geometrical reconstruction of the heart anatomy, either 3D or 4D, is usually an indispensable step.

Besides being fundamental to simulation and analysis, geometric models are also important to the visualization of complex heart anatomies. In clinical practice, medical images are mostly viewed as 2D slices or cross sections. Personalized cardiac anatomic models can be used as a complementary tool in training and patient education. Furthermore, dynamic information about the heart (e.g. blood flow behavior, myocardial motion and deformation) cannot be easily obtained from 2D cross-sectional images. Constructing a time-varying heart model not only provides important insights into the anatomical information, but also helps the physicians understand and evaluate the mechanical function of the heart. Additionally, with the rapid development of automatic segmentation techniques for cardiac imagery [7], there is a growing need for both 3D and 4D patient-specific heart model reconstruction methods.

Constructing patient-specific cardiac model is challenging: the anatomy of the heart is complex and unexpected abnormalities (e.g. holes) may occur. Many approaches have been proposed over the years to reconstruct geometric models of the heart from cardiac images. Most of the studies are focused on reconstructing heart chambers and aorta as these components are usually easier to be delineated from medical images [10]. Some reconstruction methods are image-independent, which means that the geometry is extracted from prior segmentation results (e.g. contour lines, binary segmentation masks, and point clouds) [5, 17, 27–29]. Whereas others involve segmentation and image processing (e.g. registration) in the mesh construction pipeline [11, 30, 31].

More generally, surface reconstruction methods can be broadly categorized into two major types: explicit and implicit [15]. Explicit approaches (e.g. Delaunay triangulation [3] and ball-pivoting algorithm [4]) reconstruct the data as parametric or triangulated surfaces that precisely represent the object with vertex locations. Whereas implicit approaches (e.g. marching cubes [19] and radial basis function [6]) typically define the surface as implicit functions. Readers are referred to [15] for a more detailed review on 3D surface reconstruction. Regarding 4D surface reconstruction, deformable models and statistical shape models (SSM) are widely used [5, 11, 30]. One of the challenges of these methods is that they mostly rely on prior knowledge of the shape or topology for constructing the initial model. Our method differentiates from other related algorithms as it only requires a segmentation as input and works for arbitrary topology.

Subdivision plays an important role in computer graphics for producing a smooth appearance. Starting with a coarse control mesh, new mesh elements (i.e. faces, vertices, and edges) are generated based on subdivision rules, and different levels of details can be achieved. Due to the coarse-to-fine (or multiresolution) property of subdivision surfaces, they have been widely used in areas such as animation [8], Discrete Global Grid Systems [1], and sketch-based modeling [20]. The hierarchical structure of subdivision also enables multiresolution manipulation for curves and surfaces [21, 23, 24], where the change of control mesh is reflected on the refined mesh. Additionally, the ability of modeling arbitrary topologies [25] makes subdivision surfaces suitable for reconstructing complex heart anatomy.

In this paper we present a framework for extracting temporally coherent (i.e. 1-to-1 vertex correspondence) surface models from time-varying segmented cardiac images using Loop subdivision. Using a subdivision representation allows us to create a smooth approximation and to capture details at multiple scales. The method is outlined as follows (Figure 1):

(1) From a 3D segmentation mask of one of the time frames, we construct a high-resolution mesh using marching cubes algorithm to capture all geometric details of the surface.
(2) An initial control mesh is constructed by simplifying the high-resolution mesh, and its subdivision matrix is obtained.
(3) A weighted least-squares system is constructed and solved for optimizing the control mesh. This step can be iteratively performed until a desirable threshold has been reached.
(4) After the control mesh of the current frame is optimized, we use the current control mesh as an initial mesh for the next frame. Subsequent time frames can be constructed using the same approach.

The main contribution of this method is the ability to produce temporally coherent 4D cardiac meshes which balance the visual appearance and the fitting accuracy. The novel use of subdivision surfaces in the reconstruction allows us to fit the data at a controllable resolution. Subdivision is also important in tackling the problem of topological variations.

2 RELATED WORK

Topology is one of the main challenges of heart surface reconstruction. Depending on the specific problem, simplified heart models or sophisticated topology handling can be used. In [5], the left heart model is divided into three parts (i.e. the LV sac, the Y-junction, and the connection between them) before the surface fitting. [28] assumes that the segmentation of a heart chamber is topologically equivalent to a sphere and ignores other structures such as valves. In [17], all delineation contours are mapped onto a single plane and construct meshes using Delaunay triangulation. A tree structure is then extracted to take into account the intra- and inter-frame topology changes. One of the limitations of this method is that it only works for parallel contours. Another challenge is to balance the data fitting accuracy and the visual appearance. In [27], the authors use thin plate splines (TSP) to iteratively fit an initial mesh to the contour lines and use butterfly subdivision and Laplacian smoothing to improve the visual appearance of the surface. However, the subdivision is followed by an independent coarsening step to regularize the vertex location. This loses the inherent coarse-to-fine hierarchy of subdivision surfaces and increases the computational time. Our method is similar to [11] which uses decimation, smoothing and remeshing to reconstruct a high-quality initial mesh and uses it to fit subsequent meshes. In comparison, our method constructs a coarser initial mesh and uses its subdivision to capture details in the data fitting. A more comprehensive review of cardiovascular modeling techniques is presented in [10].

3 SUBDIVISION SURFACE FITTING

In order to fit a subdivision surface to the volumetric data of a single time frame, we first construct an initial control mesh from the data, and then we model the problem as a weighted least-squares system. We fit the subdivided initial mesh to the boundary of the volumetric data by solving a linear system, from which an optimized control mesh is obtained. Figure 2 gives a high-level overview of the surface fitting process.

The first subsection introduces the datasets, followed by the details of the surface fitting process.

3.1 Data representation

The datasets we use are segmentation masks of different heart components (e.g. LV, LA, and left heart). A segmentation mask of a 3D cardiac image can be represented by a binary function $\Phi : \mathbb{N}^3 \rightarrow \{0, 1\}$,

$$\Phi(\boldsymbol{i}) = \begin{cases} 1 & inside \\ 0 & outside \end{cases},$$

where $\boldsymbol{i} \in \mathbb{N}^3$ is the index of a voxel. A signed distance transform ($D : \mathbb{N}^3 \rightarrow \mathbb{R}$) is then computed from the segmentation mask to measure the Euclidean distance of a point in space to the heart surface. The distance transform $D(\boldsymbol{i})$ of voxel $\boldsymbol{i}$ is positive if the voxel is inside the volume and negative if outside. From the discrete distance transform, we compute $d(\boldsymbol{v})$, the distance of a vertex $\boldsymbol{v}$, using tri-linear interpolation (i.e. linear interpolation along x,y,z directions).

3.2 Control mesh construction

A control mesh of a subdivision surface is the coarsest level mesh that controls the geometry of the subdivision surface. To reduce the stair-stepping effect and take advantage of the hierarchical

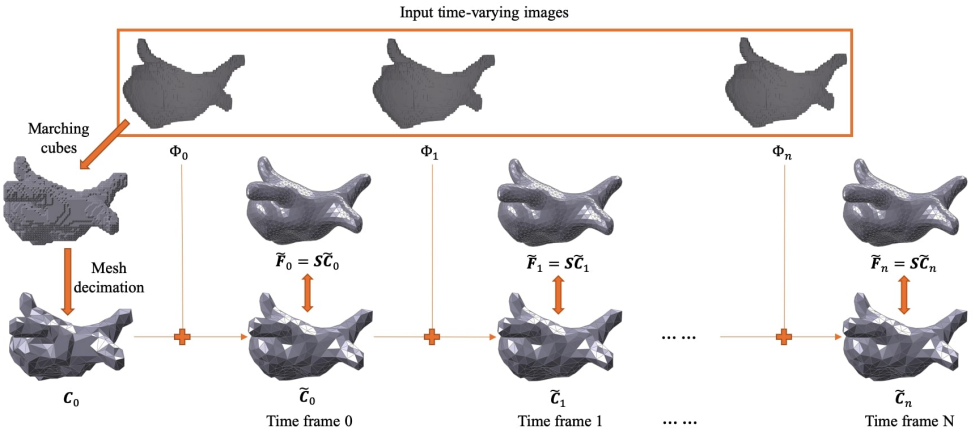

Figure 1: Time-varying subdivision surface construction. Φ_i is volumetric image of time frame i. C_0 is the initial control mesh of the first time frame. $\tilde{C}_i$ and $\tilde{F}_i$ are the optimized control mesh and refined mesh of time frame i, respectively. The initial control mesh for time frame i is $\tilde{C}_{i-1}$. S is the subdivision matrix.

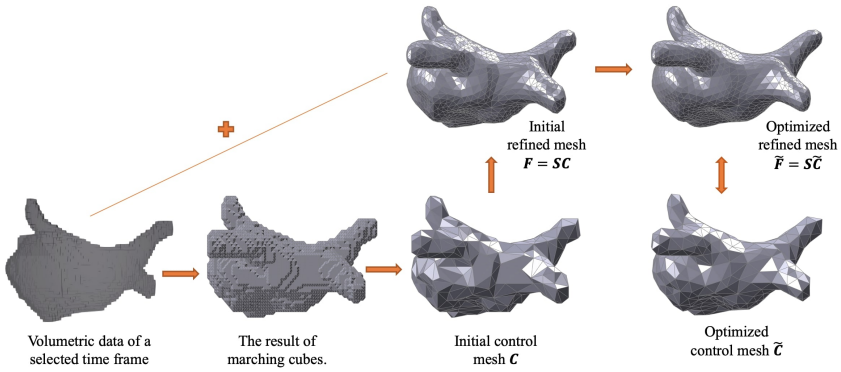

Figure 2: Subdivision surface construction for the first time frame.

structure, the control mesh should be coarse and have the same topology as the volumetric data. In order to capture topological details of the data in the control mesh, we first construct a high-resolution mesh using the marching cubes. We then apply an edge-collapsing mesh decimation algorithm to reduce the number of polygons on the dense mesh [14]. Given an appropriate decimation rate, the simplified mesh (denoted by C) will have the same topology and will keep important geometry details of the original data (Figure 2).

3.3 Mesh optimization

Once the initial control mesh C is obtained, it is deformed to better fit the volumetric data. This surface fitting process is controlled by two terms: error and tension. The error term maintains the closeness of the mesh to the boundary, while the tension term maintains the fairness and smoothness of the mesh.

3.3.1 Error term. The error energy determines how close the current mesh is to the boundary. It acts as an external force to "pull" the vertices toward the boundary. For each vertex $\boldsymbol{v}$, we want to minimize its distance to the boundary of the volume (i.e. its distance transform $d(\boldsymbol{v})$). The per-vertex error is determined by $e(\boldsymbol{v}) = ||d(\boldsymbol{v})||^2$,) We define the error term as the summation of all vertex errors. The error term of a mesh $\boldsymbol{M} = (V, E)$ is $E(\boldsymbol{M}) = \sum_{\boldsymbol{v}_i \in V} ||d(\boldsymbol{v_i})||^2$. Since the distance transform is a scalar field (i.e. the magnitude of the external force), we use the unit vertex normal $\hat{\boldsymbol{n}}(\boldsymbol{v})$ to determine the direction of the external force. Assume $\boldsymbol{V'}$ is the vertex set after the mesh evolving (the edge connection is not changed during surface fitting), the error term is minimized when

$$\boldsymbol{V'} = V + \boldsymbol{N}(V), \tag{1}$$

where

$$\boldsymbol{N} = \begin{bmatrix} d(\boldsymbol{v}_1)\hat{\boldsymbol{n}}(\boldsymbol{v}_1) \\ d(\boldsymbol{v}_2)\hat{\boldsymbol{n}}(\boldsymbol{v}_2) \\ \vdots \\ d(\boldsymbol{v}_m)\hat{\boldsymbol{n}}(\boldsymbol{v}_m) \end{bmatrix}.$$

3.3.2 Tension term. The tension energy determines how smooth and fair the current mesh is. It acts as an internal force that redistributes the vertices to 'unfold' the mesh and to avoid triangles that

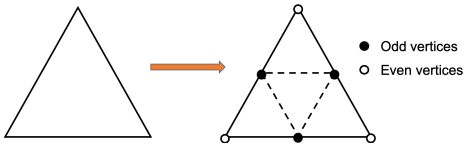

Figure 3: Illustration of Loop subdivision. Each triangle face on the mesh is split into 4 new faces. After face splitting, the odd vertices (i.e. the new vertices on each original edge) and the even vertices (i.e. the old vertices) will be re-positioned based on different rules.

are too skinny and stretched. Mesh Laplacian [9] has been used for improving mesh smoothness and fairness. For each vertex, a tension force is computed as a vector from its current position to the center of its neighbors:

$$\boldsymbol{L}(\boldsymbol{v}_i) = \frac{1}{valence(\boldsymbol{v}_i)} \sum_{(i,j)\in \boldsymbol{E}} \boldsymbol{v}_j - \boldsymbol{v}_i.$$

The tension term of a mesh $\boldsymbol{M} = (\boldsymbol{V}, \boldsymbol{E})$ is $T(\boldsymbol{M}) = \sum_{\boldsymbol{v}_i \in \boldsymbol{V}} ||L(\boldsymbol{v}_i)||^2$. The tension term is minimized when

$$\boldsymbol{LV'} = 0, \tag{2}$$

where

$$L_{ij} = \begin{cases} \frac{1}{valence(v_i)} & \text{if } (i,j) \in \boldsymbol{E}, \\ -1 & \text{if } i = j, \\ 0 & \text{otherwise.} \end{cases}$$

3.4 Surface fitting

The initial control mesh is fitted by iteratively minimizing the two constraints. The optimization is an over-determined system which is solved in a least-squares sense. In order to capture the details, we use the refined mesh to minimize the energy and to get an optimized coarse mesh.

3.4.1 Least-squares system. From the energy minimization equations (1) and (2), we obtain an over-determined system:

$$\begin{bmatrix} \boldsymbol{L} \\ \boldsymbol{I} \end{bmatrix} \boldsymbol{V'} = \begin{bmatrix} 0 \\ \boldsymbol{V} + \boldsymbol{N}(\boldsymbol{V}) \end{bmatrix}.$$

We can assign different weights W_T and W_E to the error and tension terms:

$$\begin{bmatrix} W_T \boldsymbol{L} \\ W_E \end{bmatrix} \boldsymbol{V'} = \begin{bmatrix} 0 \\ W_E(\boldsymbol{V} + \boldsymbol{N}(\boldsymbol{V})) \end{bmatrix}. \tag{3}$$

The solution is the minimizer of

$$W_T^2 ||\boldsymbol{LV'}||^2 + W_E^2 \sum_i ||\boldsymbol{v}_i + d(\boldsymbol{v})\hat{\boldsymbol{n}}(\boldsymbol{v}_i) - \boldsymbol{v}_i'||^2.$$

Note that W_T and W_E are constants that determines how important the tension and error terms are. Based on our experiments, the combination of $W_T = 1$ and $W_E = 0.25$ ensures a good visual appearance and a good fit to the data. Table 1 depicts the effect of different weights: a larger tension weight produces a smoother mesh, while a larger error weight makes the mesh closer to the data and reduces the mesh smoothness.

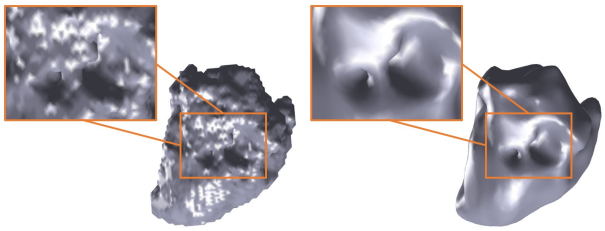

Figure 4: The left atrium with a hole. Left: marching cubes mesh. Right: our method with one level of subdivision. Dataset is obtained from [26].

3.4.2 Loop subdivision matrix. Loop subdivision is a subdivision scheme that is designed for triangle meshes. Loop subdivision is a generalization of cubic B-spline subdivision, and it has C^2 continuity at regular vertices (i.e. valence of six). The subdivision process is composed of two steps: face splitting and vertex re-positioning. As depicted in Figure 3, each triangle face on the mesh is split into 4 new faces. The 3 new vertices on the original edges are called "odd vertices", and the 3 old vertices are "even vertices". Each vertex are then re-positioned based on the subdivision masks proposed in [18].

Subdivision is a coarse-to-fine approach, where the refined mesh can be represented by the product of a subdivision matrix and the coarse mesh. Let $\boldsymbol{C}$, $\tilde{\boldsymbol{C}}$, $\boldsymbol{F}$ and $\tilde{\boldsymbol{F}}$ be the vertex sets of the initial control mesh, optimized control mesh, initial refined mesh, and optimized refined mesh, respectively. Then, we have

$$\begin{cases} \boldsymbol{F} = \boldsymbol{SC} \\ \tilde{\boldsymbol{F}} = \boldsymbol{S}\tilde{\boldsymbol{C}} \end{cases},$$

where $\boldsymbol{S}$ is the subdivision matrix. The subdivision matrix can be computed when the vertices are iteratively subdivided, and it can represent any level of subdivision. For instance, let $\boldsymbol{C}^0$ be the vertex set of the control mesh and $\boldsymbol{C}^{\boldsymbol{i}}$ be the vertex set after the i-th iteration of subdivision. Then $\boldsymbol{C}^i = \boldsymbol{S}_i \boldsymbol{C}^{i-1}$, $i = 1, 2, \cdots$, where $\boldsymbol{S}_i$ is the subdivision matrix of the i-th iteration. Thus, the vertex set after n levels of subdivision is $\boldsymbol{C}^n = \boldsymbol{S}_n \boldsymbol{S}_{n-1} \cdots \boldsymbol{S}_1 \boldsymbol{C}^0 = \boldsymbol{SC}^0$, where $\boldsymbol{S} = \boldsymbol{S}_n \boldsymbol{S}_{n-1} \cdots \boldsymbol{S}_1$ represents the collective subdivision matrix of the entire process. Since the subdivision matrix is sparse, the computation can be done efficiently, and the result can be saved for subsequent time frames. From equation (3), we derive the linear system for the subdivision fitting:

$$\begin{bmatrix} W_T \boldsymbol{L}(\boldsymbol{F}) \\ \boldsymbol{W}_E \end{bmatrix} \tilde{\boldsymbol{F}} = \begin{bmatrix} 0 \\ \boldsymbol{W}_E(\boldsymbol{F} + \boldsymbol{N}(\boldsymbol{F})) \end{bmatrix}$$

$$\Rightarrow \begin{bmatrix} W_T \boldsymbol{L}(\boldsymbol{F})\boldsymbol{S} \\ \boldsymbol{W}_E \boldsymbol{S} \end{bmatrix} \tilde{\boldsymbol{C}} = \begin{bmatrix} 0 \\ \boldsymbol{W}_E(\boldsymbol{F} + \boldsymbol{N}(\boldsymbol{F})) \end{bmatrix}, \tag{4}$$

where $\boldsymbol{L}$ is the mesh Laplacian obtained from the refined initial mesh, and $\boldsymbol{N}(\boldsymbol{F})$ is the scaled vertex normal of the initial refined mesh. The optimized control mesh $\tilde{\boldsymbol{C}}$ is found by solving equation (4) in a least-squares sense.

4 TIME-VARYING SURFACE

The subdivision surface fitting method in Section 3 can be used to efficiently reconstruct time-varying datasets. As depicted in Figure

Table 1: Demonstration for different parameters. In each of (b)-(f), the left is the control mesh and the right is the result after one level of subdivision, optimized using the corresponding weights. Dataset is obtained from [26].

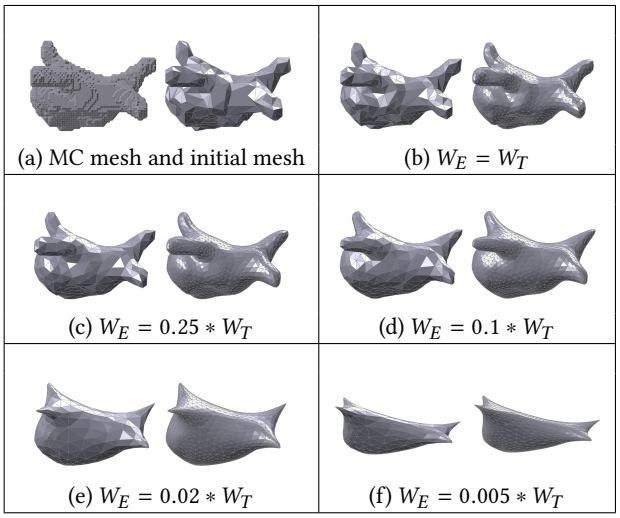

1, given a set of time-varying volumes $\{\Phi_0, \Phi_1, ..., \Phi_n\}$, the goal is to construct a sequence of control meshes $\{\tilde{C}_0, \tilde{C}_1, ..., \tilde{C}_n\}$ such that their corresponding subdivided meshes $\{\tilde{F}_0, \tilde{F}_1, ..., \tilde{F}_n\}$ are optimized with respect to the volumes. Since the difference between two consecutive volumes is not significant (i.e. a slight change in the geometry and no change in the topology), we only need to construct one initial control mesh for the first time step, and then use the optimized control mesh as the initial control mesh for the optimization in the next time step. This not only helps to keep the topological constancy, but also improves the performance. The process of constructing $\tilde{C}_i$ is as follows, where C_i denotes the initial control mesh to be fitted at time step i:

(1) If $i = 0$, then construct C_i by mesh decimation, otherwise, $C_i = \tilde{C}_{i-1}$,
(2) Compute the mesh Laplacian L_i and the scaled vertex normal N_i based on the subdivided initial control mesh $F_i = SC_i$,
(3) Solve $\begin{bmatrix} W_T L_i S \\ W_E S \end{bmatrix} \tilde{C}_i = \begin{bmatrix} 0 \\ W_E(SC_i + N_i) \end{bmatrix}$ for $\tilde{C}_i$.

Figure 1 depicts the pipeline for time-varying subdivision surface construction. The resulting coarse mesh sequence has vertex-to-vertex correspondence between the time steps, which can be easily interpolated to produce quality animation.

5 RESULTS AND DISCUSSION

Since MC is a widely used surface reconstruction algorithm in the field of medicine and since many other methods are built on top of MC [11, 30, 31], we compare our method to MC in the quantitative evaluation. We have applied our method to multiple datasets for different heart components. Table 2 compares our method and the MC method in terms of mesh resolution and least-squares error. The result is based on four datasets: normal left atrium (LA1), left atrium with a hole (LA2), left heart with the aorta (LH), and one time frame from a 30-frames time-varying left ventricle (LV). Since these datasets are segmented pieces of the entire heart, we use the their bounding boxes to represent their sizes (in terms of number of voxels along x, y, z directions). From the comparison, we note that our surface has less number of faces than MC while our least-squares error remains low. The result indicates that our method is able to construct high-quality meshes (in terms of accuracy and smoothness) with lower mesh resolution. Figures in Table 1 and Figure 4 show visual comparisons between MC and our method. In Table 1, the optimized subdivision mesh ((c) right) well-approximates the volumetric data and captures important details. The optimized mesh significantly reduces the jaggedness in the MC mesh ((a) left). Figure 4 shows that the topology unchanged (i.e. the hole) in our mesh, while the surface is smoother than the MC construction.

Table 2: Compare our method with marching cubes. Column $\#F_{MC}$ and $\#F_{ours}$ are the number of faces of the marching cubes mesh and our mesh, respectively. Column $\bar{E}_{MC}$ and $\bar{E}_{ours}$ are the average per-vertex least-squares errors.

Data	Size	$\#F_{MC}$	$\#F_{ours}$	$\bar{E}_{MC}$	$\bar{E}_{ours}$
LA1	60*83*48	14168	2832	0.431	0.346
LA2	56*74*44	14296	5144	0.499	0.297
LH	69*32*60	8114	2592	0.981	0.906
LV	67*24*55	7944	1904	0.827	0.530

Table 3: Evaluation of the mesh stair-stepping effect. Columns VP_{MC} and VP_{ours} are the number of total vertex pairs in the meshes constructed by marching cubes and our method. Columns h_{MC} and h_{ours} are the coplanar ratios of MC mesh and ours.

Data	VP_{MC}	VP_{ours}	h_{MC}	h_{ours}
LA1	21252	4248	45.61%	0.66%
LA2	21444	7713	41.43%	2.81%
LH	12170	3888	25.07%	0.23%
LV	11908	2856	58.58%	5.25%

In order to quantitatively evaluate the mesh jaggedness (stair-stepping effect), we have used the quadric error metrics (QEM). The QEM method was first proposed by Garland [12] for mesh simplification. The error quadric Q for a vertex v is a 4×4 symmetric matrix that depicts the distance of a point in space to v's neighboring faces. For each valid vertex pair (v_i, v_j) (i.e. connected by an edge), we compute the cost of the vertex contraction $(v_i, v_j) \rightarrow \bar{v}$ using the quadratic error: $E_{i,j} = \bar{v}^\top (Q_i + Q_j)\bar{v}$. The target point $\bar{v}$ is selected from v_i, v_j, and their midpoint such that it has the lowest cost. The one-ring neighborhoods of v_1 and v_2 are considered coplanar if $E_{i,j} < \epsilon$ (we use $\epsilon = 1e-06$). The jaggedness can be measured by the ratio of coplanar vertex pairs ($VP_{coplanar}$) to the total vertex pairs (VP):

$$h = \frac{VP_{coplanar}}{VP}.$$

A lower coplanar ratio indicates less stair-stepping effect. Table 3 compares the coplanar ratios of the marching cubes and our

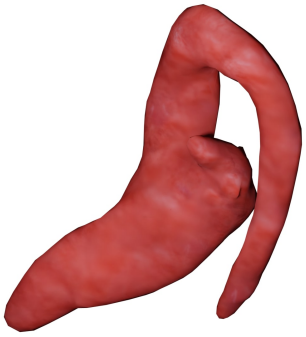

Figure 5: Reconstruction of the left heart and the aorta surface.

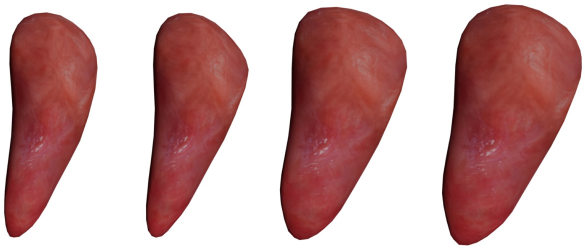

Figure 6: Four time frames of a reconstructed left ventricle animation.

method on four datasets. The results show that the coplanar ratio of marching cubes reconstruction is higher than that of our method. Our subdivision surface significantly reduces the stair-stepping effect of the marching cubes mesh.

Our method can be used to create more visually-appealing results by attaching textures. Figure 5 shows a textured result of a reconstructed left heart surface (including left atrium, left ventricle, and the aorta). Figure 6 shows four time frames from the animation of a left ventricle during diastole. The time-varying data comes from the segmentation masks of 4D Flow MRI images over the entire cardiac cycle. The data originally consists of 30 time frames, from which we fit 30 temporally coherent meshes (i.e. having the same vertex connectivity) using the method described in Section 4. An animation with higher temporal resolution is then generated by linear interpolation. Thanks to the 1-to-1 vertex correspondence, a single synthetic texture can be mapped to all time frames.

6 CONCLUSION AND FUTURE WORK

We presented a method for fitting subdivision surfaces to segmented time-varying cardiac images. The method produces smooth, hierarchical subdivision surfaces while maintaining the reconstruction accuracy. The evaluation demonstrates that our surface model is able to reconstruct the segmented data with fewer polygons while reducing the jaggedness. We have also shown that it works for arbitrary topology and preserves 1-to-1 vertex correspondence in the time-varying model.

As future work, the twisting motion (or torsional motion) of the heart could be incorporated in the reconstruction. As proposed by [5], manually placed landmarks and control points can be added to take into account the torsion on the myocardium surface. Furthermore, we can adopt semi- and fully-automatic segmentation tools in the future to make it a complete pipeline for visualizing time-varying cardiac images.

ACKNOWLEDGMENTS

We thank Huang-Li Jason Chen for inspiring us to use subdivision surfaces in heart modeling. We also thank the Natural Sciences and Engineering Research Council of Canada (NSERC) for funding this work [grant number: NSERC CRD 478365-2014, sponsor Circle CVI].

REFERENCES

[1] Troy Alderson, Ali Mahdavi-Amiri, and Faramarz Samavati. 2016. Multiresolution on spherical curves. *Graphical Models* 86 (2016), 13 – 24. https://doi.org/10.1016/j.gmod.2016.05.002

[2] Kathleen D. Ang, Faramarz F. Samavati, Samin Sabokrohiyeh, Julio Garcia, and Mohammed S. Elbaz. 2019. Physicalizing cardiac blood flow data via 3D printing. *Computers & Graphics* 85 (2019), 42–54. https://doi.org/10.1016/j.cag.2019.09.004

[3] Franz Aurenhammer, Rolf Klein, and Der-Tsai Lee. 2013. *Voronoi Diagrams and Delaunay Triangulations* (1st ed.). World Scientific Publishing Co., Inc., USA.

[4] F. Bernardini, J. Mittleman, H. Rushmeier, C. Silva, and G. Taubin. 1999. The ball-pivoting algorithm for surface reconstruction. *IEEE Transactions on Visualization and Computer Graphics* 5, 4 (1999), 349–359. https://doi.org/10.1109/2945.817351

[5] Federico Canè, Benedict Verhegghe, Matthieu Beule, Philippe Bertrand, Rob van der Geest, Patrick Segers, and Gianluca De Santis. 2018. From 4D Medical Images (CT, MRI, and Ultrasound) to 4D Structured Mesh Models of the Left Ventricular Endocardium for Patient-Specific Simulations. *BioMed Research International* 2018 (01 2018), 1–14. https://doi.org/10.1155/2018/7030718

[6] J. C. Carr, R. K. Beatson, J. B. Cherrie, T. J. Mitchell, W. R. Fright, B. C. McCallum, and T. R. Evans. 2001. Reconstruction and Representation of 3D Objects with Radial Basis Functions. In *Proceedings of the 28th Annual Conference on Computer Graphics and Interactive Techniques (SIGGRAPH '01)*. Association for Computing Machinery, New York, NY, USA, 67–76. https://doi.org/10.1145/383259.383266

[7] Chen Chen, Chen Qin, Huaqi Qiu, Giacomo Tarroni, Jinming Duan, Wenjia Bai, and Daniel Rueckert. 2020. Deep Learning for Cardiac Image Segmentation: A Review. *Frontiers in Cardiovascular Medicine* 7 (2020), 25. https://doi.org/10.3389/fcvm.2020.00025

[8] Tony DeRose, Michael Kass, and Tien Truong. 1998. Subdivision Surfaces in Character Animation. In *Proceedings of the 25th Annual Conference on Computer Graphics and Interactive Techniques (SIGGRAPH '98)*. Association for Computing Machinery, New York, NY, USA, 85–94. https://doi.org/10.1145/280814.280826

[9] Mathieu Desbrun, Mark Meyer, Peter Schröder, and Alan H. Barr. 1999. Implicit Fairing of Irregular Meshes Using Diffusion and Curvature Flow. In *Proceedings of the 26th Annual Conference on Computer Graphics and Interactive Techniques (SIGGRAPH '99)*. ACM Press/Addison-Wesley Publishing Co., USA, 317–324. https://doi.org/10.1145/311535.311576

[10] Alejandro Frangi, W.J. Niessen, and Max Viergever. 2001. Three-dimensional modeling for functional analysis of cardiac images: A review. *IEEE transactions on medical imaging* 20 (02 2001), 2–25. https://doi.org/10.1109/42.906421

[11] Mingchen Gao, Junzhou Huang, Shaoting Zhang, Zhen Qian, Szilard Voros, Dimitris Metaxas, and Leon Axel. 2011. 4D Cardiac Reconstruction Using High Resolution CT Images. In *Functional Imaging and Modeling of the Heart*, Dimitris N. Metaxas and Leon Axel (Eds.). Springer Berlin Heidelberg, Berlin, Heidelberg, 153–160.

[12] Michael Garland and Paul S. Heckbert. 1997. Surface Simplification Using Quadric Error Metrics. In *Proceedings of the 24th Annual Conference on Computer Graphics and Interactive Techniques (SIGGRAPH '97)*. ACM Press/Addison-Wesley Publishing Co., USA, 209–216. https://doi.org/10.1145/258734.258849

[13] Richard Gray and Pras Pathmanathan. 2018. Patient-Specific Cardiovascular Computational Modeling: Diversity of Personalization and Challenges. *Journal of cardiovascular translational research* 11 (04 2018), 80–88. https://doi.org/10.1007/s12265-018-9792-2

[14] Hugues Hoppe. 1996. Progressive Meshes. In *Proceedings of the 23rd Annual Conference on Computer Graphics and Interactive Techniques (SIGGRAPH '96)*. Association for Computing Machinery, New York, NY, USA, 99–108. https://doi.org/10.1145/237170.237216

[15] A. Khatamian and Hamid Arabnia. 2016. Survey on 3D Surface Reconstruction. *Journal of Information Processing Systems* 12 (01 2016), 338–357. https://doi.org/10.3745/JIPS.01.0010

[16] Gaoyang Li, Haoran Wang, Mingzi Zhang, Simon Tupin, Aike Qiao, Youjun Liu, Makoto Ohta, and Hitomi Anzai. 2021. Prediction of 3D Cardiovascular hemodynamics before and after coronary artery bypass surgery via deep learning. *Communications Biology* 4 (01 2021). https://doi.org/10.1038/s42003-020-01638-1

[17] Chi Lim, Yi Su, Si Yeo, Gillian Ng, Vinh-Tan Nguyen, Liang Zhong, Ru San Tan, Kian Keong Poh, and Ping Chai. 2014. Automatic 4D Reconstruction of Patient-Specific Cardiac Mesh with 1-to-1 Vertex Correspondence from Segmented Contours Lines. *PloS one* 9 (04 2014), e93747. https://doi.org/10.1371/journal.pone.0093747

[18] Charles T. Loop. 1987. *Smooth Subdivision Surfaces Based on Triangles.* Master's thesis. Department of Mathematics, University of Utah.

[19] William E. Lorensen and Harvey E. Cline. 1987. Marching Cubes: A High Resolution 3D Surface Construction Algorithm. *SIGGRAPH Comput. Graph.* 21, 4 (Aug. 1987), 163–169. https://doi.org/10.1145/37402.37422

[20] A. Nasri, W. Bou Karam, and F. Samavati. 2009. Sketch-Based Subdivision Models. In *Proceedings of the 6th Eurographics Symposium on Sketch-Based Interfaces and Modeling* (New Orleans, Louisiana) *(SBIM '09)*. Association for Computing Machinery, New York, NY, USA, 53–60. https://doi.org/10.1145/1572741.1572751

[21] Luke Olsen, Faramarz Samavati, and Richard Bartels. 2007. Multiresolution for curves and surfaces based on constraining wavelets. *Computers & Graphics* 31 (06 2007), 449–462. https://doi.org/10.1016/j.cag.2007.01.033

[22] Alberto Redaelli and Emiliano Votta. 2020. Cardiovascular patient-specific modeling: Where are we now and what does the future look like? *APL Bioengineering* 4 (12 2020), 040401. https://doi.org/10.1063/5.0031452

[23] Javad Sadeghi and Faramarz Samavati. 2009. Technical Section: Smooth reverse subdivision. *Computers and Graphics* 33 (06 2009), 217–225. https://doi.org/10.1016/j.cag.2009.03.012

[24] Javad Sadeghi and Faramarz F. Samavati. 2011. Smooth Reverse Loop and Catmull-Clark Subdivision. *Graph. Models* 73, 5 (Sept. 2011), 202–217. https://doi.org/10.1016/j.gmod.2011.03.004

[25] Faramarz Samavati, Nezam Mahdavi-Amiri, and Richard Bartels. 2000. Multiresolution Surfaces Having Arbitrary Topologies by a Reverse Doo Subdivision Method. *Computer Graphics Forum* 21 (07 2000). https://doi.org/10.1111/1467-8659.00572

[26] Catalina Tobon-Gomez, Arjan J. Geers, Jochen Peters, Jürgen Weese, Karen Pinto, Rashed Karim, Mohammed Ammar, Abdelaziz Daoudi, Jan Margeta, Zulma Sandoval, Birgit Stender, Yefeng Zheng, Maria A. Zuluaga, Julian Betancur, Nicholas Ayache, Mohammed Amine Chikh, Jean-Louis Dillenseger, B. Michael Kelm, Saïd Mahmoudi, Sébastien Ourselin, Alexander Schlaefer, Tobias Schaeffter, Reza Razavi, and Kawal S. Rhode. 2015. Benchmark for Algorithms Segmenting the Left Atrium From 3D CT and MRI Datasets. *IEEE Transactions on Medical Imaging* 34, 7 (2015), 1460–1473. https://doi.org/10.1109/TMI.2015.2398818

[27] Benjamin Villard, Vicente Grau, and Ernesto Zacur. 2018. Surface Mesh Reconstruction from Cardiac MRI Contours. *Journal of Imaging* 4 (01 2018), 16. https://doi.org/10.3390/jimaging4010016

[28] Oskar Škrinjar and Arnaud Bistoquet. 2009. Generation of Myocardial Wall Surface Meshes from Segmented MRI. *Journal of Biomedical Imaging* 2009, Article 23 (Jan. 2009), 10 pages. https://doi.org/10.1155/2009/313517

[29] Min Wan, Wei Huang, Jun-Mei Zhang, Xiaodan Zhao, Ru San Tan, Xiaofeng Wan, and Liang Zhong. 2015. Variational Reconstruction of Left Cardiac Structure from CMR Images. *PLOS ONE* 10, 12 (12 2015), 1–17. https://doi.org/10.1371/journal.pone.0145570

[30] Xiaoxu Wang, Viorel Mihalef, Zhen Qian, Szilard Voros, and Dimitris Metaxas. 2012. 3D cardiac motion reconstruction from CT data and tagged MRI. In *2012 Annual International Conference of the IEEE Engineering in Medicine and Biology Society*. IEEE, San Diego, California, 4083–4086. https://doi.org/10.1109/EMBC.2012.6346864

[31] Shaoting Zhang, Xiaoxu Wang, Dimitris Metaxas, Ting Chen, and Leon Axel. 2009. LV surface reconstruction from sparse tMRI using Laplacian Surface Deformation and Optimization. In *2009 IEEE International Symposium on Biomedical Imaging: From Nano to Macro*. IEEE, Boston, MA, 698–701. https://doi.org/10.1109/ISBI.2009.5193143